

## Power estimation for four wheeled skid steered robot prototype

Shawki Abouel-seoud<sup>1</sup>, Youssef Akhnouk<sup>1,\*</sup>, Mohamed Abdelrahman<sup>1</sup>,  
Nabil Hammad<sup>1</sup>

<sup>1</sup>Department of Automotive and locomotive, faculty of engineering, Helwan University, Cairo, Egypt

\*Corresponding author

**ABSTRACT:** This Paper shows power consumption study of electric vehicle prototype and provides a technique to overcome the limitation of the power source capacity. Design and building a prototype for electric vehicle with the proper sensors is discussed for the power analysis purposes. Deployment embedded system to drive the prototype in a specific path is presented. The sensors readings are deployed in the skid steered vehicle kinematic model for estimating power consumption characteristics. A control strategy for the embedded system is suggested to minimize the electric power consumption without motion trajectory deviation. The introduced prototype is a self-driving vehicle where the main controller is handling all driving requirements without human interfering.

**Index Terms:** Power analysis, skid steering, kinematic model, electric vehicle.

Date of Submission: 25-09-2020

Date of acceptance: 07-10-2020

### I. INTRODUCTION

Electric vehicles are considered as a potential solution for reducing the emissions affecting the climate change where it uses power source with zero carbon dioxide emissions, so that it is expected by 2030 around 14% of the vehicles will be electrically powered [1].

Skid steering is a steering technique in which the outer radius wheels of the vehicle rotates faster than the inner radius wheels along the maneuver curve, the inner wheels can be stopped to minimize the curvature radius or can be rotated in reverse direction then the vehicle rotates around itself. Skid steering is characterized by compactness, light mass and requires few mechanical parts so that the mechanical setup is simple and costs less than the other complicated ordinary mechanical steering systems[2].Skid steering is widely used in heavy vehicles like loader or military tanks as it is characterized by mechanical simplicity, saves the volume occupied by the ordinary steering parts and needs less maintenance and can be easily controlled just by controlling the speeds of the electric motors driving the wheels.

Analyzing the Power consumption is important for driving electric vehicles due to the limitation in the power source capacity as mentioned in [3]. The effect of the deployed control technique has been investigated in [4] during driving the vehicle and how it maintains the power consumption within save limits while climbing a hill. A power consumption prediction model has been presented in [5], which deploys wheel speeds, ground friction coefficient and vehicle load in the mathematical model then comparing the simulation results with a real electric vehicle power consumption, where the vehicle has been driven over different ground types and loads along an 8 shape path. Coulomb and friction models have been deployed to simulate the induced electric motors torque and power in [6], where both models are deployed in power prediction and comparing between them. The real time current measurements have been carried out using two current sensors to calculate the electric motors induced torque and power to compare between them and the simulated induced power from the mathematical models. It was found that the skid steered vehicle kinematic model is important for carrying out the vehicle power analysis based on the wheels measured rotating speeds and motors induced current. The skid steered wheels are considered as simple tracks in many theoretical and experimental studies [7], where the wheels rotating speeds are considered to be equal for each vehicle side along the experiment time. On the other hand, the asynchronous model for the four wheeled skid steered vehicle is not considered widely because the complexity of the model. Each wheel of the model has its own rotating speed in the asynchronous model. For this study the multi continuously variable rotating speed for each wheel is more suitable, therefor it is used in developing the kinematic model in [8][9].

This article is prepared as following, section II introduces the kinematic model of a skid steered four wheeled vehicle by which the longitudinal and the rotational speeds of the vehicle can be estimated, section III introduces the used prototype with the sensors deployed to measure the rotational speeds of the wheels and the flowing current in the motors in real time, section IV shows the used embedded system to move the prototype in specific path and save the measured data from the sensors, Section V shows the used rules to convert the measured wheels' rotational speed and motors' current into electrical power and energy, section VI shows the applied experimental tests, also shows the measured wheels' rotational speed and the motors' flowing current during motion in the specified paths. By applying the rules of sections II and V the linear and the rotational speed of the vehicle, the power consumption, wheels torque and the consumed energy are estimated, section VII introduces the conclusion and the future work

## II. KINEMATIC MODEL

In this study, a kinematic model for the skid steered four wheeled vehicle is used to find out the linear longitudinal vehicle speed. It is assumed that no friction between the wheels and the contact ground to simplify the mathematical model. In this model, four electric motors and attached to the four wheels to drive them along the given path. The wheels speeds are continuously controlled and monitored through a set of speed sensors, which fixed on the wheels. According to the segment type in the path, the embedded system is driving the wheels and simultaneously measures and stores the speeds, current and battery voltage for power analysis purposes. The assumed motion trajectory can be deviated from the actual trajectory. In this study, it is assumed they are identical to minimize the deviation between the measured parameters and the calculated motors power and torque. For more understanding, a general layout for the experimental setup is shown in Fig.1 where the main components and the basic dimensions are presented. In the presented model, the coordinates are assumed to be fixed to the vehicle body.

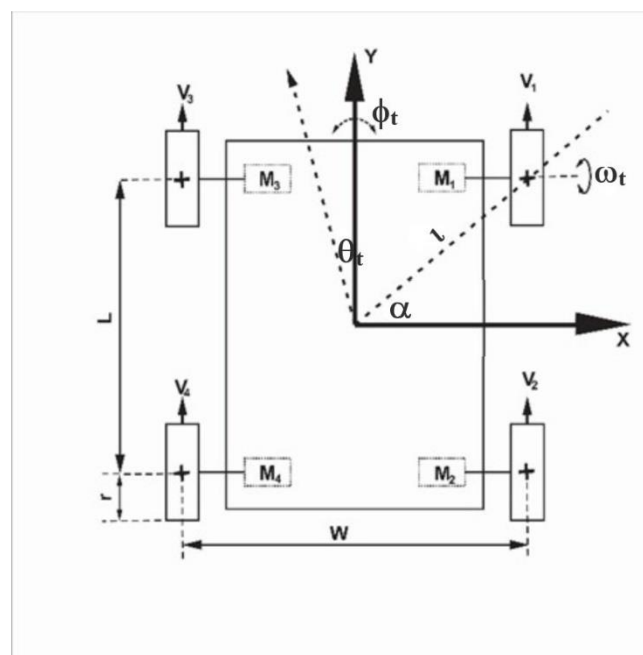


Fig.1.kinematic model

Fig.1 is the model of a skid steered vehicle with four motors, each motor is connected to a wheel with radius  $r$  rotating with rotational speed  $\omega_t$ , based on Eq.(1), the average tangential speed of the wheel  $v_t$  is expressed in Eq.(2).

$$v_t = r \cdot \omega_t, \tag{1}$$

$$v_t = \frac{r}{4} \sum_{i=1}^4 \omega_t^i, \tag{2}$$

where  $i$  is the wheels index and  $r$  is assumed to be equal for all wheels.

The wheels rotational speeds are considered to be in clockwise direction and therefore they are positive values but in case of counterclockwise direction are negative values, so that the vehicle differential velocity  $\hat{v}_t$  is written as in Eq.(3).

$$\hat{v}_t = r(\omega_t^1 + \omega_t^2 - \omega_t^3 - \omega_t^4), \tag{3}$$

while the vehicle rotational speed around the perpendicular axis to the vehicle body  $\phi_t = d\theta_t/dt$  where  $\theta_t$  is the heading angle of the vehicle, to get the rotational speed in the terms of the wheels rotational speed is expressed in Eq.(4),  $t$  refers to the time.

$$\phi_t = \frac{\hat{v}_t \cos(\alpha)}{l}, \tag{4}$$

$\cos(\alpha)$  and  $l$  can be solved geometrically as shown in Eq.(5) and Eq.(6), then the vehicle rotational speed is driven and shown in Eq.(7).

$$l = \frac{\sqrt{W^2+L^2}}{2}, \tag{5}$$

$$\cos(\alpha) = \frac{W}{2l}, \tag{6}$$

$$\phi_t = \frac{\hat{v}_t r W}{W^2+L^2}, \tag{7}$$

A. State and Control Vectors

The state vector  $\xi_t$  is shown in Eq.(8)

$$\dot{\xi}_t = A . u_t, \tag{8}$$

where  $u_t$  is the control vector of the system related to the direct kinematics model  $u_t = (v_t, \phi_t)$ . From Eq.(2) and Eq.(7),  $u_t$  can be driven and presented in Eq.(9); Where  $\Omega_t$  is a vector of the wheels velocities in Eq.(10).

$$u_t = \begin{pmatrix} r/4 & r/4 & r/4 & r/4 \\ rW & rW & -rW & -rW \\ W^2+L^2 & W^2+L^2 & W^2+L^2 & W^2+L^2 \end{pmatrix} . \Omega_t, \tag{9}$$

$$\Omega_t = \begin{pmatrix} \omega_t^1 \\ \omega_t^2 \\ \omega_t^3 \\ \omega_t^4 \end{pmatrix}, \tag{10}$$

then the state vector  $\xi_t$  can be expressed as in Eq.(11).

$$\xi_t = \begin{pmatrix} \dot{x} \\ \dot{y} \\ \dot{\theta} \end{pmatrix} = \begin{pmatrix} \cos \theta_t & 0 \\ \sin \theta_t & 0 \\ 0 & 1 \end{pmatrix} . u_t. \tag{11}$$

III. PROTOTYPE

In this section, the skid steered vehicle prototype is presented. The main parts of the prototype such as the motors, sensors and the embedded system are declared in order to highlight the combination between the real experimental setup and the calculated parameters from the measured signals of the attached sensors and how the embedded system is handling them.



Fig.2. The prototype

Fig.2 shows the used prototype made to perform the experimental tests consists of four electric motors each attached to a wheel and two 12 volts batteries connected in series to feed the motors with electric power.

Each motor is operated by a motor driver (MD10C), which supports PWM signal to control the rotation speed and the direction of rotation for each motor individually.

Four speed sensors, from the optical type, are mounted on the four wheels to deliver the wheels rotation speeds in the real time during the experiment. Four current sensors (Allegro ACS712), are Hall effect type sensors, are integrated with the motors drivers to measure the induced current in real time.

Ultrasonic sensor, HCSR04 module, is attached to the prototype frontal area to detect obstacles but more sensors must be mounted to achieve this purpose. In this study, the ultrasonic sensor is deployed to examine the control algorithm. The main part in the deployed embedded system is the Arduino (ATmega2560) which collects the data from the sensors and handle the control signals to the motor drivers. The sensors must be calibrated before carrying out the real time experiment to achieve high accuracy measurements.

#### IV. CONTROL STRATEGY

According to NHTSA-The National Highway Traffic Safety Administration, the autonomous vehicle definition is a vehicle which can be operated without any driver interference [10].The following control strategy is an event-based controller which has feedback from sensors, but the current and speed sensors are used for measurement purposes only. The controller receives signals from the speed and the current sensors every second and controls the speed and the operating period of the motors by sending pulse width modulated (PWM) signals continuously to the motor drivers beside that storing the collected data from the sensors in the SD card module to save it as presented in Fig. 3. The deployed control algorithm during the vehicle operation is that the controller sends control signals to the motor drivers and starts internal timer, which can be paused in case of obstacle appears in front of the prototype and is detected by the ultrasonic sensor. The motion is resumed by removing the obstacle as shown in the presented flowchart in Fig. 4.

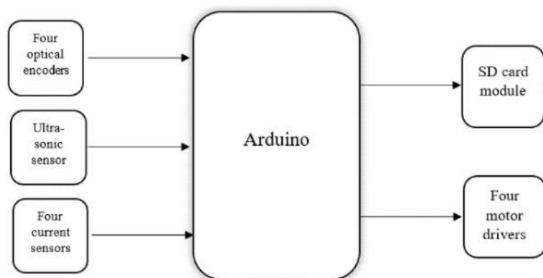


Fig. 3. System layout

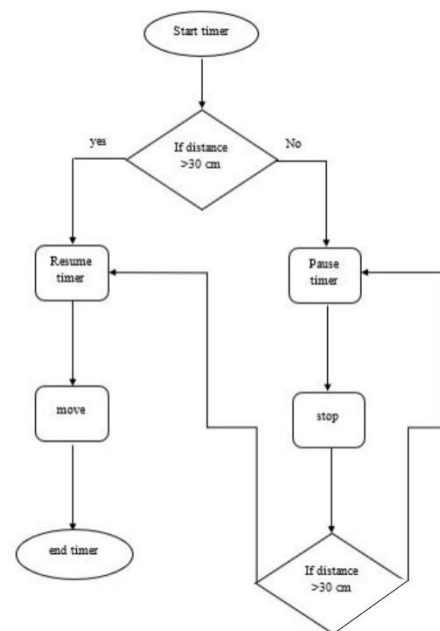


Fig. 4. control algorithm

#### V. POWER ANALYSIS

The linear speed of the vehicle is calculated as a function in the rotational speed and wheel radius as shown in Eq.(12). The rotational speed is measured by an optical encoder (speed sensor) and the measured radius of the wheel is found to be 0.27 m.

$$v_t = r \cdot \omega_t, \tag{12}$$

where  $v_t$  is the wheel's tangential speed in m/s,  $\omega_t$  is the wheel's rotational speed in rad/sec of the wheel and  $r$  is the wheel radius in m. Hence the sensor speed readings are in rpm, then the Eq.(13) is used to convert the readings into to rad/sec

$$\omega_t = \frac{2 \cdot \pi \cdot n}{60}, \tag{13}$$

where  $n$  is the rotational speed in rpm; and the liner speed in km/hr is calculated from Eq.(14)

$$v_t = \frac{3.6 * 2 * \pi * n * r}{60}. \tag{14}$$

The electrical power of the motor in watt is driven from Eq.(15), where  $V$  is the voltage drop across the motor external terminals in volt and  $I$  is the current flows through motor's winding in ampere. Also, Eq.(15) is considered as input electric power for each motor used in the vehicle.

$$P = V * I, \tag{15}$$

torque of the wheel is calculated from Eq.(16)

$$P = T * \omega_m, \tag{16}$$

where  $T$  is the resultant torque in N.m. and  $\omega_m$  is the rotational speed of the electric motor in rad/sec.-since the motor is connected to the wheel directly, then their rotational speeds are equal  $\omega_m = \omega_t$ , the mechanical efficiencies of the motor  $\eta_m$  and the gear box  $\eta_{gb}$  are considered in Eq.(17).

$$P * \eta_m * \eta_{gb} = T * \omega_t, \tag{17}$$

From Eq.(15) and Eq. (17), then

$$T * \omega_t = V * I * \eta_m * \eta_{gb}, \tag{18}$$

$$T = \frac{V * I * \eta_m * \eta_{gb}}{\omega_t}. \tag{19}$$

By converting the rotational speed from  $n$  in rpm, that measured by speed sensor, into  $w$  in rad/sec by the aid of Eq.(13), so that the Torque in N.m. can be driven from Eq.(20)

$$T = \frac{60 * V * I * \eta_m * \eta_{gb}}{2 * \pi * n}, \tag{20}$$

energy consumed in watt.hr. can be driven from Eq.(21)

$$E = P * t, \tag{21}$$

where  $P$  is the input electric power in watt and  $t$  is the experiment duration time for each segment in the trajectory in hr. The mechanical efficiency of the motor, as presented in the technical data sheet [11] is a function of the torque. Since the torque is not measured, then it can be estimated from the technical data sheet as a function in motor speed. From the presented curve in the technical data sheet [11] and using motor rotational speed, the torque and then the efficiency are estimated. Also, the mechanical efficiency can be found by following the same procedure as mentioned previously by using the technical data sheet of the used electric motor by deploying gearbox rotational speed. The measured rotational speed is after the reduction ratio of the gearbox, so to find out the rotational speed of the motor, Eq.(22) is used.

$$\omega_m = \omega_{gb} * R_R, \tag{22}$$

where  $\omega_m$  is the motor's rotational speed,  $\omega_{gb}$  is the gearbox's rotational speed and  $R_R$  is the gearbox reduction ratio. After disassembling the gear box attached to the electric motor, it is found that the gearbox consists of two reduction gears stages and with total reduction ratio of 44.73 as shown in Fig. 5.

All two reduction stages gearbox from this type has efficiency  $\eta_{gb}$  equals 0.81. After getting the reduction ratio, then the motor efficiency can be drawn as a function in the gearbox rotational speed as shown in Fig. 6.



Fig. 5. Two stages gearbox with 44.73 reduction ratio

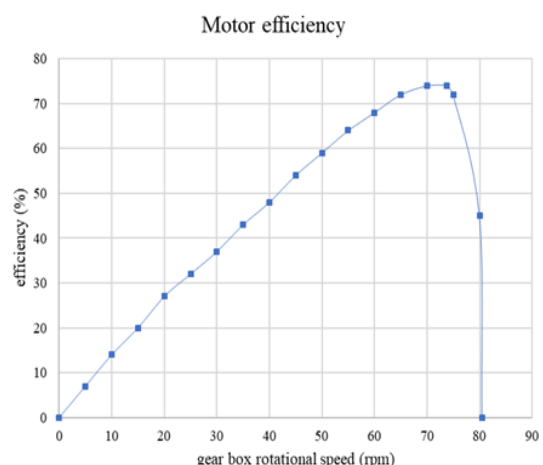


Fig. 6. Motor mechanical efficiency as a function of gearbox rotational speed

## VI. EXPERIMENTAL TESTS

Fig.7. The proposed trajectory shows the proposed trajectory where the vehicle moves along the trajectory and all the fixed sensors send their readings to the central control unit. The central control unit processes the inputs from the sensor and records them along the time of the experiment. The purpose of the tests is estimating the forces acting on the wheels during both of longitudinal motion and cornering motion.

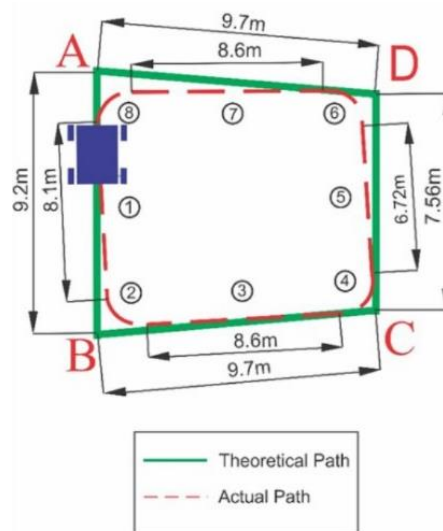


Fig.7. The proposed trajectory

The target is to experiment the vehicle behavior in the cornering motion and notice the difference between the signals of the sensors at the longitudinal motion and cornering motion.

### A. Single Counterclockwise Cornering

The vehicle starts at point A, as shown in Fig.7, heading forward to point B then heads counterclockwise to point C. Fig. 8 shows the linear speeds of the wheels during single counterclockwise cornering movement, at the standby segment, wheels rotational speeds are zero rpm. Wheels speeds start to rise during the longitudinal motion in segment (1) then when the cornering motion in segment (2) begins, both of the front left wheel and the rear left wheel rotational speeds fall down to the minimum value of 5 rpm, while the front right wheel and the rear right wheel increase to the maximum value of the rotation speeds of 53 and 52 rpm respectively. This great difference in the rotational speed of the left and right sides wheels lead to the cornering motion. All the wheels' speeds change again to be almost equal when the longitudinal motion in segment (3) starts and then fall to zero in the standby segment.

Fig. 9 shows the current flows through motors windings during a single cornering movement to the left. In the cornering motion segment (2), the current of the front left motor reaches to the minimum value which equals -0.53 ampere and -0.43 ampere for the rear left motor, while the current of the front right motor reaches its maximum current which equals 1.5 ampere and 1.91 for the rear right motor. The negative current is considered as a regenerative brake current, where the electric motor works as a generator the electric current flows from the motor to the attached battery, but in this case, the electric circuits are not ready to retrieve the induced power from the motor. while the large current induced in the motors in the left side of the vehicle is due to operating the vehicle at high speed meanwhile the motors in the right side are turned off by applying zero volt as an input. Fig. 10 shows the vehicle linear speed during the test, to have zero km/hr in the first standby segment, rises in the longitudinal segment (1), increases to have a peak value of 3.3 km/hr in the cornering segment (2), then falls in the longitudinal segment (3) and decreases to zero km/hr again in the last standby segment. Fig. 11 displays the rotational speed of the vehicle across the entire test. Starts with zero rad/second in the first standby segment, then fluctuates when the longitudinal segment (1) starts, rises to have a peak value of 0.74 rad/second in the cornering segment (2), then falls in the longitudinal segment (3) and finally reaches zero rad/second in the last standby segment.

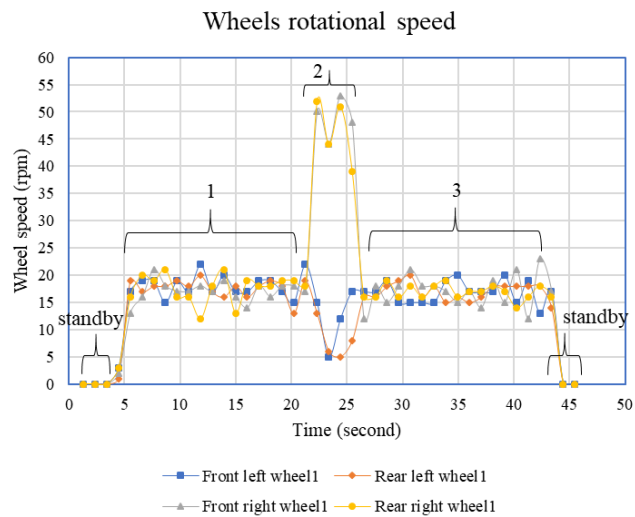


Fig. 8. Rotational speed of the wheels during a single counterclockwise cornering

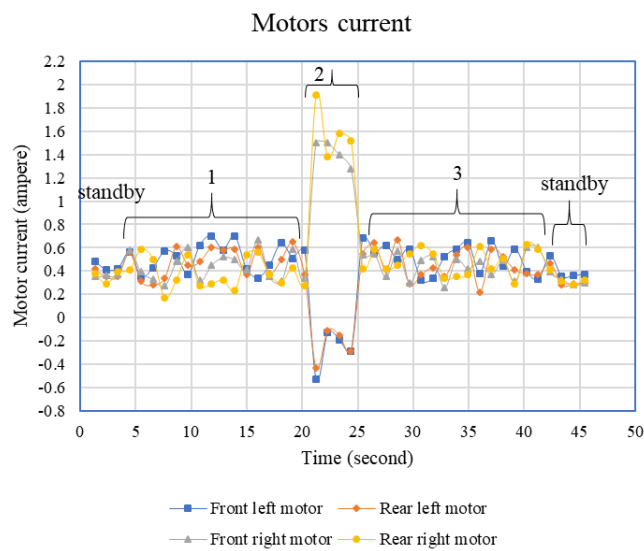


Fig. 9. Electric current flows through the motors during a single counterclockwise cornering

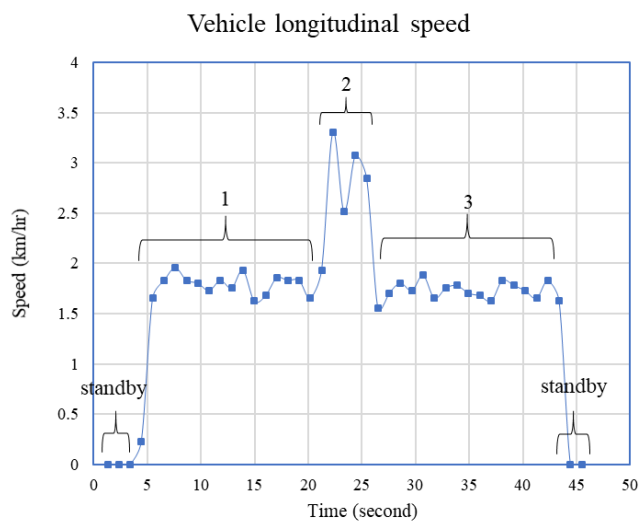


Fig. 10. Vehicle longitudinal speed at single counterclockwise cornering movement test

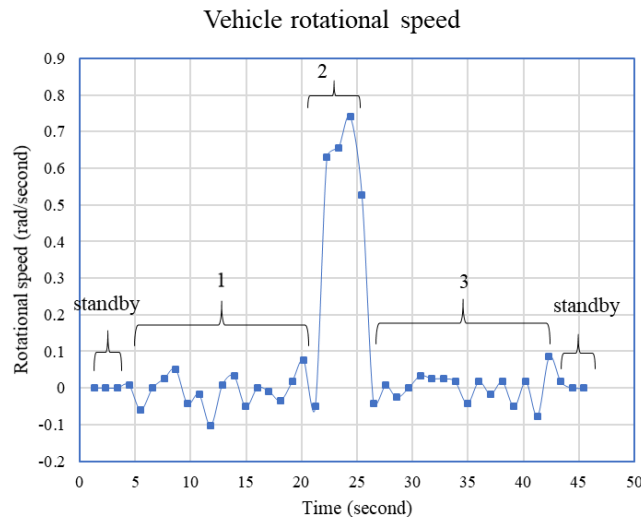


Fig. 11. Vehicle rotational speed at single counterclockwise cornering movement test

The input voltage a cross motors terminal during the planned cornering is 18.7 volt while the vehicle is driven at high speed during the longitudinal motion experiment. But after deployment of this input voltage, it is found that the cornering angle is large, to decline the cornering angle, two solutions have been examined. First solution is increasing the duration period of the experiment, while the vehicle is doing the cornering. But this solution does not show any improvement in the large cornering angle. The second solution is increasing the input voltage along the duration time of the experiment to equal 19.2 volt and this solution leads to a reasonable cornering angle.

The designed vehicle has a time-based-controller, which means a presetting for the time is determined for each segment of the trajectory in the control program, to drive the vehicle. The normal timer of the Arduino mega controller, deployed in the designed vehicle, cannot handle the obstacle interrupts coming from the ultrasonic sensor installed in the vehicle. So that another timer has been deployed which can be paused until the obstacle is removed. This timer sets 1 second as the minimum period can be controlled.

Fig. 12 shows the electrical power of the motors during the experiment. The front left and the rear left motors induce power of zero watt during the cornering motion in segment (2). On the other hand, the front right motor induces power of 28.8 watt and the rear right motor induces power equals 36.6 watt. These values are the power peaks as shown in Fig. 12. The front left motor and rear left motor, in this situation, are working as electric generators. They induce power to the battery, but the necessary electric circuits (voltage sensors) are not installed. There are current flows, but the voltage drop is assumed to be zero, Therefore the resultant power appears as zero. Installing the necessary electric circuits and voltage sensors to make use of the induced power from the motors are recommended as apart from the future work.

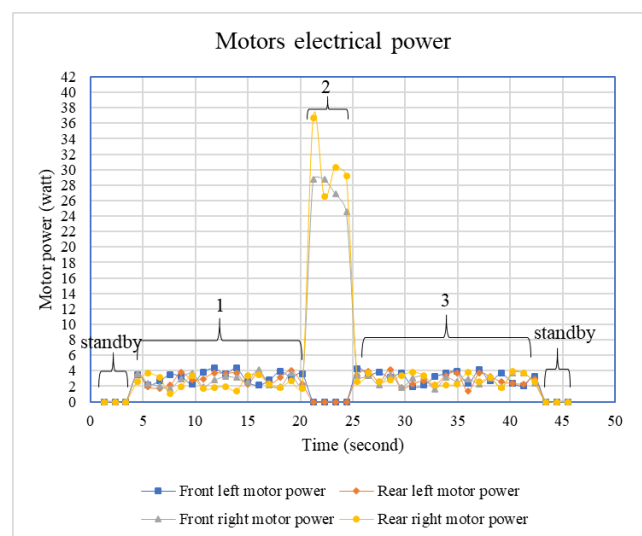
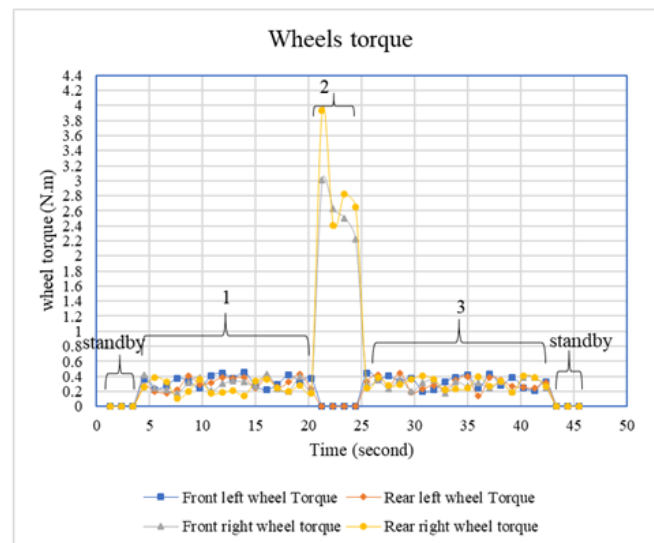


Fig. 12. Electrical power of the motors during the single left cornering



**Fig. 13.** Torque applied at the wheels during the single left cornering

**Fig. 13** shows the torque applied at wheels during the experiment, similar to the previously analyzed induced power, the applied torque at both of the front left and the rear left wheels equals zero N.m during the cornering segment where the estimated torque is a function in the induced power. But the peak value of the applied torque at the front right wheel equals 3 N.m and at the rear right wheel equals 3.9 N.m.

#### B. Single clockwise Cornering

The vehicle starts at point B and is heading to point A then turns clockwise to the point D. **Fig. 14** shows the rotational speed of the wheels during single right cornering. The linear speed equals zero at standby segment. By beginning of the experiment, it rises during the longitudinal motion in segment (1). In the cornering segment (8), the rotation speed of the front left wheel reaches the peak value equals 50 rpm while the rear right wheel reaches 48 rpm as a peak value. Meanwhile the front right wheel speed drops down to 4 rpm and the rear right wheel speed drops down to 1 rpm. All the rotational speeds of the wheels are showing a similar average value during the longitudinal motion in segment (7) and drop down again to zero in the last standby segment.

**Fig. 15** shows the electric current flows through motors windings during the experiment. The front left wheel motor shows a peak current at 1.26 ampere, the rear left wheel motor shows a peak current at 1.4 ampere in the cornering segment (8). The front right wheel motor reaches a minimum value of -0.68 ampere and the rear right wheel motor lowest current value is -1.05 ampere. The peak current of the wheel's motors in this part from the experiment is lower than the previous one, but the regenerated currents are higher than the previous part because of the ground declination.

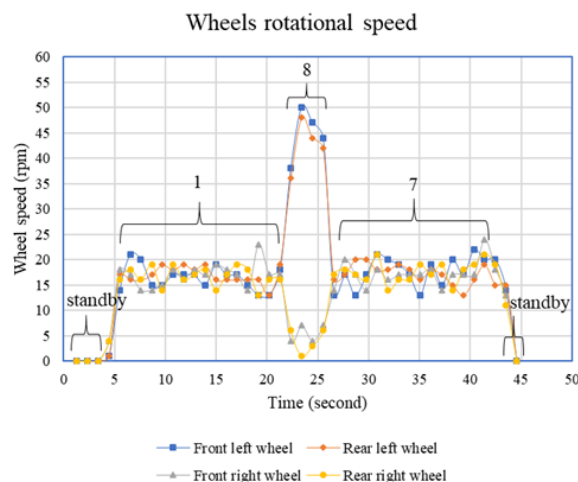


**Fig. 14.** Wheels rotational speed during single clockwise cornering

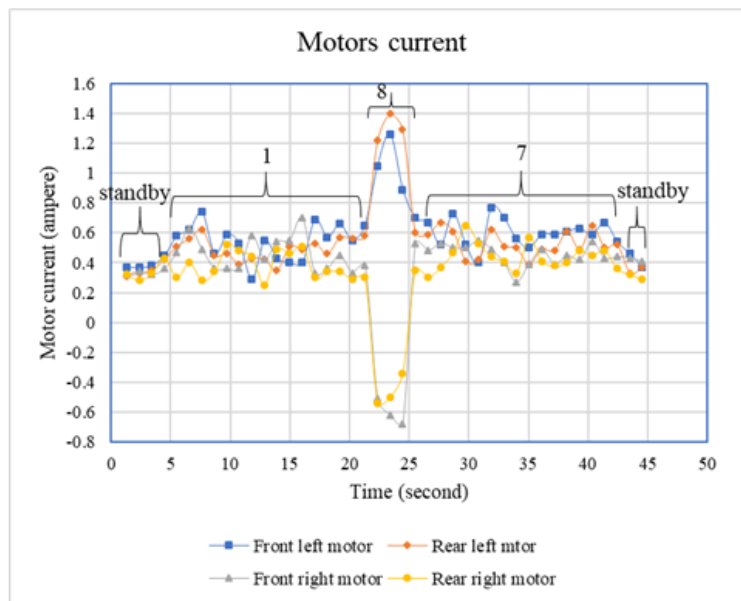


Fig. 15. Motors electric current during single right cornering

Fig. 16 shows the linear speed of the vehicle across the entire test, at the beginning the speed is zero in the standby segment then rises when the longitudinal segment (1) starts, highly increase when the cornering segment (8) begins to have a peak value of 2.7 km/hr then falls when the longitudinal segment (7) begins and finally drops to zero km/hr in the standby segment. Fig.17 represents the rotational speed of the vehicle throughout the test, the rotational speed equals zero rad/second in the first standby segment, fluctuates around zero in the longitudinal segment (1), drops to a minimum value of -0.77 rad/second in the cornering segment (8), then rises to fluctuate around zero and equals zero rad/second in the last standby segment.

The rotational speed in the cornering segment (8) is a negative value as it is in clockwise direction while the counterclockwise is considered as the positive direction of the rotation.

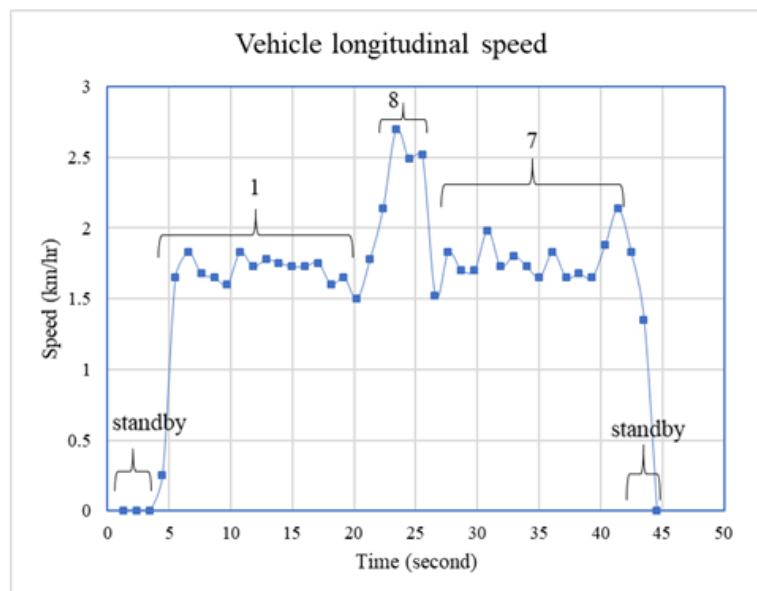


Fig. 16. Vehicle longitudinal speed at single clockwise cornering movement test

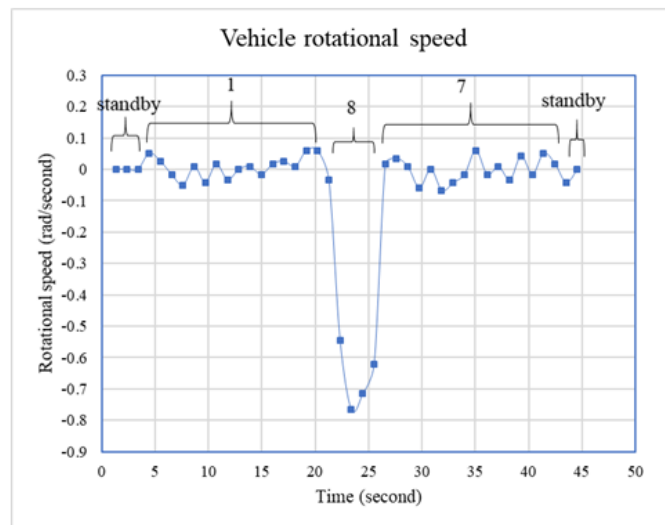


Fig. 17. Vehicle rotational speed at single clockwise cornering movement test

Fig. 18 displays the output electrical power of the motors during the experiment during cornering segment (8). The output power from the front left wheel motor reaches a peak power at 24.1 watt and the highest output power for the rear left wheel motor is 26.88 watt. The front right and the rear right wheels motors deliver output power equals zero watt due to the reasons explained before. Meanwhile the applied torque at the front left wheel reaches a peak value at 2.2 N.m and at the right left wheel equals 2.46 N.m as a maximum torque value during the cornering segment (8) as shown in Fig. 19.

C. Single Cornering Experiment's Electrical Energy Consumption

The consumed electrical energy by the vehicle and by each motor during a single left cornering movement are shown in Table 1. A comparison between the counterclockwise cornering and clockwise cornering from the energy consumption point of view is carried on and presented in Fig.20. Notice that the titles of the x axis is the number of the segment; the left number indicates the counterclockwise cornering segments and the right number indicates the clockwise cornering segments experiment. It is clear from Fig. 20, that the electrical energy consumption during the counterclockwise cornering segments are higher than the clockwise cornering segments. Because of the electric current peak values during the counterclockwise cornering segments are higher than those of the clockwise cornering segments as the floor may be inclined a little bet which resists the turn in the counterclockwise direction.

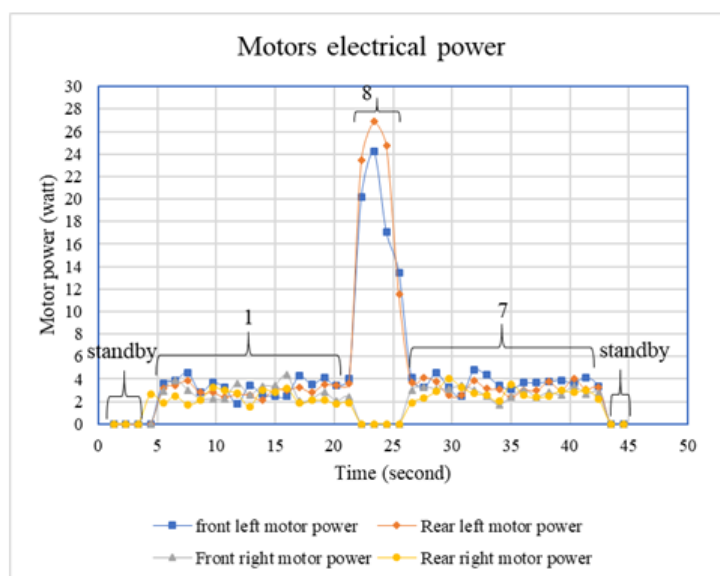


Fig. 18. Electrical output power of the motors during single right cornering

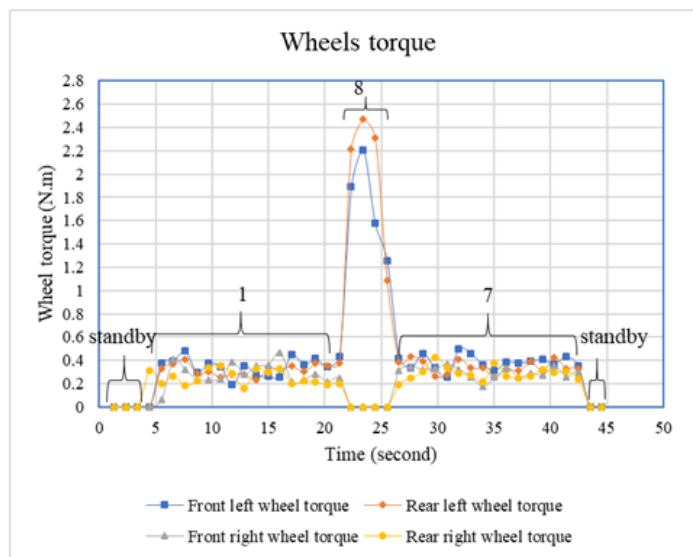


Fig. 19. The applied torque at the wheels during single right cornering

Table 1. Motors electrical energy consumption in watt.hr and vehicle electrical energy consumption in watt.hr/km for a single left cornering

Energy Segment	Front left motor (watt.hr)	Rear left motor (watt.hr)	Front right motor (watt.hr)	Rear right motor (watt.hr)	Total energy (watt.hr)	Energy consumption (watt.hr/km)
Longitudinal motion (1)	0.0141	0.0129	0.0120	0.0103	0.04954	6.1171
Cornering motion (2)	0	0	0.0238	0.0268	0.0507	18.1107
Longitudinal motion (3)	0.0148	0.0133	0.0132	0.0138	0.0553	6.4307
sum	0.0289	0.0263	0.0491	0.0510	0.1555	30.6586

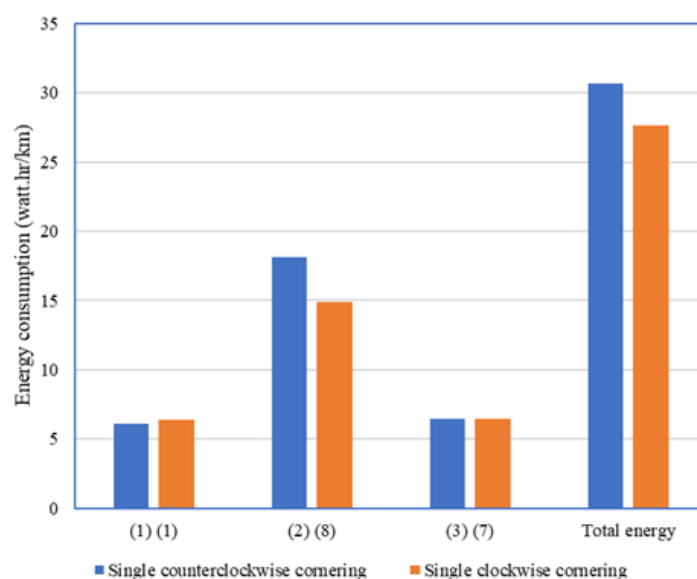


Fig.20. Electrical energy consumption in a single cornering

## VII. CONCLUSIONS

Time based controller succeeded in controlling the vehicle to move within the proposed path and in maintaining the electric energy consumption within the save limits for such trajectory. More enhancement for the energy and the motion controller are required for achieving more accurate vehicle behavior in these fields. Further experiments must be carried out to determine the needed time to cover a specific distance or turn. It is found that the prototype covers the same distance in different time intervals by changing the contact ground type, where the friction coefficient is not taken in consideration in this study. The effect of the friction coefficient appears clearly during the turns, where the slippage of the wheels increases rapidly. A new controller must be introduced to control the wheels rotation speeds precisely during the cornering motion to maintain the correct required turning angle along the cornering curvature, that assists in reducing the losses in the electrical energy and power consumption along the specified trajectory. A new control algorithm must be introduced to reduce the consumed power, which appears to be higher in case of cornering motion in comparison to the longitudinal motion, where the PID or similar classical controller algorithms can help in avoiding the excessive power consumption.

## NOMENCLATURE

$v_t$	Vehicle Linear speed
$\omega_t$	Wheels rotational speed
$r$	Wheel radius ( $r=0.27$ m)
$i$	Wheel's index
$\phi_t$	Rotational speed of the vehicle
$\theta_t$	Heading angle of the vehicle
$l$	Distance between vehicle's center of gravity and wheel's center of gravity
$\alpha$	Angle of inclination of $l$
$\xi$	State vector
$u_t$	Control vector
$\Omega_t$	Wheels velocity vector
$W$	Vehicle track ( $W= 0.86$ m)
$L$	Vehicle wheelbase ( $L= 0.8$ m)
$P$	Power
$V$	Voltage
$I$	Current
$T$	Torque
$t$	Time
$E$	Energy
$R_R$	Gear box reduction ratio ( $R_R= 44.73$ )
$\omega_m$	Motor's rotational speed
$\omega_{gb}$	Gearbox's rotational speed

## REFERENCES

- [1] S. Fukushima, P. Stief, J. Dantan, A. Etienne, and A. Siadat, "Scenario Analysis of Car- and Ride- Sharing Services Based on Life Cycle Simulation," *Procedia CIRP*, vol. 80, pp. 328–333, 2018, doi: 10.1016/j.procir.2019.01.051.
- [2] V. Nazari and M. Naraghi, "A vision-based intelligent path following control of a four-wheel differentially driven skid steer mobile robot," *2008 10th Int. Conf. Control. Autom. Robot. Vision, ICARCV 2008*, no. December, pp. 378–383, 2008, doi: 10.1109/ICARCV.2008.4795549.
- [3] J. Morales *et al.*, "Power Analysis for a Skid-Steered Tracked Mobile Robot," 2006.
- [4] M. I. Yacoub, D. S. Neculescu, and J. Z. Sasiadek, "Experimental Evaluation of Energy Optimization Algorithm for Mobile Robots in Three-dimension Motion Using Predictive Control," *21st Mediterr. Conf. Control Autom. Chania*, pp. 437–443, 2013.
- [5] J. L. Mart, A. Mandow, A. Peque, and A. Garc, "Simplified Power Consumption Modeling and Identification for Wheeled Skid-Steer Robotic Vehicles on Hard Horizontal Ground," *2010 IEEE/RSJ Int. Conf. Intell. Robot. Syst.*, pp. 4769–4774, 2010.
- [6] W. Yu, E. Collins, and O. Chuy, *Mobile Robots - Current Trends*. 2011.
- [7] T. Wang, Y. Wu, J. Liang, C. Han, J. Chen, and Q. Zhao, "Analysis and Experimental Kinematics of a Skid-Steering Wheeled Robot Based on a Laser Scanner Sensor," *Sensors*, vol. 15, no. 5, pp. 9681–9702, 2015, doi: 10.3390/s150509681.
- [8] E. Martínez-García and R. Torres-Córdoba, "4WD skid-steer trajectory control of a rover with spring-based suspension analysis: Direct and inverse kinematic parameters solution," *Lect. Notes Comput. Sci. (including Subser. Lect. Notes Artif. Intell. Lect. Notes Bioinformatics)*, vol. 6424 LNAI, no. PART 1, pp. 453–464, 2010, doi: 10.1007/978-3-642-16584-9\_44.
- [9] E. A. Martínez-García, O. Mar, and R. Torres-Cordoba, "Dead-reckoning inverse and direct kinematic solution of a 4W independent driven rover," *2010 IEEE ANDESCON Conf. Proceedings, ANDESCON 2010*, pp. 1–6, 2010, doi: 10.1109/ANDESCON.2010.5633569.
- [10] NHTSA, "Automated driving systems."
- [11] Dunkermotoren, "D.C. Motors," 2000. [Online]. Available: [www.akcesoria-cnc.pl/pdf/silniki\\_dc\\_dunkermotoren.pdf](http://www.akcesoria-cnc.pl/pdf/silniki_dc_dunkermotoren.pdf).

Youssef Akhnoukh, et. al. "Power estimation for four wheeled skid steered robot prototype." *American Journal of Engineering Research (AJER)*, vol. 9(10), 2020, pp. 19-31.